Influence of thermal stratification on the transport of polydispersed expiratory particles

Monka, Aleksandra; Fraga, Bruño; Soper, David; Hemida, Hassan

DOI:
10.1063/5.0163971

Document Version
Publisher's PDF, also known as Version of record

Citation for published version (Harvard):
Monka, A, Fraga, B, Soper, D & Hemida, H 2023, 'Influence of thermal stratification on the transport of polydispersed expiratory particles', *Physics of Fluids*, vol. 35, no. 10, 103304. https://doi.org/10.1063/5.0163971

RESEARCH ARTICLE | OCTOBER 04 2023

Influence of thermal stratification on the transport of polydispersed expiratory particles

Aleksandra Monka ; Bruño Fraga ; David Soper ; Hassan Hemida

Physics of Fluids 35, 103304 (2023)
https://doi.org/10.1063/5.0163971

Physics of Fluids ARTICLE pubs.aip.org/aip/pof

Influence of thermal stratification on the transport of polydispersed expiratory particles

Cite as: Phys. Fluids **35**, 103304 (2023); doi: 10.1063/5.0163971
Submitted: 20 June 2023 · Accepted: 16 September 2023 ·
Published Online: 4 October 2023

Aleksandra Monka, Bruño Fraga,[a] David Soper, and Hassan Hemida

AFFILIATIONS

School of Engineering, University of Birmingham, Edgbaston, Birmingham B15 2TT, United Kingdom

Note: This paper is part of the special topic, Flow and the Virus.
[a]**Author to whom correspondence should be addressed:** b.fraga@bham.ac.uk

ABSTRACT

The fluid dynamics of expiratory events are complex, and understanding how indoor air conditions affect this and the spread of exhaled material is crucial to the prevention of large-scale spread of diseases. It is known that thermal stratification can trap contaminants in the lower levels of a room; however, there is a lack of studies that investigate the influence of vertical temperature gradients on the transport of expiratory particles at room scale. To this effect, we used Eulerian–Lagrangian large-eddy simulations to investigate the effect of thermal stratification on the transport of polydispersed expiratory particles during speaking in two different sized rooms. Cases with increasing temperature gradient were compared to an isothermal base case, and the influence of stratification on the exhalation jet and the particles suspended within is analyzed. The particle volume fraction was computed to quantify the spatiotemporal evolution of different particle size categories. Our results show that thermal stratification leads to an increased concentration of aerosols in the breathing zone and extends their forward reach. Aerosols up to a size threshold between 12 and 20 μm are locked up at different heights by stratification—beyond this threshold, they fall out continuously. In all cases, aerosols <20 μm traveled up to 4 m from the source, showing that physical distancing guidelines alone may be inadequate for controlling cross-infection risk for long-term exposures. Particles >60 μm are unaffected by stratification and do not follow a ballistic trajectory, falling out within 0.5 m of the infectious individual in all cases.

I. INTRODUCTION

The COVID-19 pandemic caused by the SARS-CoV-2 virus highlighted the importance of indoor air quality on the exposure to and transmission of respiratory diseases in indoor spaces. During an expiratory event, a multiphase (gas and liquid particles) buoyant turbulent cloud is released in which particles of various sizes are suspended. These expiratory particles exhibit different physical behaviors based on their size; larger particles are mostly unaffected by the cloud, while smaller particles remain suspended within it for long periods of time and follow air currents.[1–3] This turbulent cloud therefore extends the distance that particles suspended within it can travel from the infectious person. Many factors affect the behavior of expiratory particles, and it has been suggested that the distinction between aerosol and droplet particles should be made based on their physical behavior instead of the 5 μm cutoff point, which from a physics perspective has been shown to be incorrect.[3,4] In this paper, we do not assume *a priori* the size cutoff between aerosol and droplet behavior. We use the term aerosol to describe any particle that remains suspended in the air and follows air currents, and the term droplet is to describe any particle that falls out of the exhalation jet quickly and is therefore removed from the air.

Despite calls earlier in the pandemic to recognize airborne transmission of SARS-CoV-2,[5] initial guidance to reduce its spread focused on preventative measures against droplet transmission. The belief that only droplets were responsible for transmission at close range does not take into consideration that both small and large expiratory particles are most concentrated close to the source.[3,4,6] Therefore, exposure to aerosols also occurs in this region via the airborne route and evidence has shown that this can be the dominant route for pathogen transmission close to the infected individual.[7,8] Airborne transmission was first given attention in the long range to explain how people could become infected without having direct or close contact with each other.[9] Since the pandemic started, there have been many studies pointing toward airborne transmission being the dominant route in the transmission of SARS-CoV-2[9–14] and advice to reduce its spread began to be updated to include the importance of ventilation in indoor spaces to tackle the build-up of pathogens in the air.

Understanding of the modes and mechanisms of respiratory pathogen transmission and the factors affecting them is crucial to the prevention of large-scale spread of disease. The fluid dynamics of expiratory events are complex, and the spatiotemporal variations and turbulent mixing of expiratory particles need to be captured well to reflect reality. Computational fluid dynamics (CFD) has been used in the past to predict expiratory particle transport, including studies based on the Lattice Boltzmann method applied to expiratory particles or ventilation[15–18] as an alternative to the standard Navier–Stokes CFD solvers. Most studies rely on Reynolds-averaged Navier–Stokes (RANS) models,[19–27] which are not ideal to predict turbulent mixing due to reliance on isotropic turbulence closures and focus on the mean flow field. In the RANS approach, all turbulent length scales are modeled, not resolved, and only mean flow features can be obtained.[28] In the unsteady RANS (URANS) method, an unsteady term is added to the momentum equation; however, URANS still cannot capture the internally induced fluctuations of the flow field,[28] which are important in the transport of pollutants. In contrast, the large-eddy simulation (LES) approach directly resolves the larger energy-containing eddies, while eddies with a length scale smaller than the computational mesh are modeled using a sub-grid scale (SGS) model.[29] LES results are unsteady; therefore, the fluctuations in the flow field are resolved, which allows the transient features and process of turbulent mixing and fluctuations to be captured. This is an important driver of particle and pollutant dispersion; therefore, LES is able to produce more accurate results for dispersion and concentration distribution fields when compared to RANS or URANS,[28,30] although this method does require more computational resources and time. Wang and Chen[31] compared RANS, LES, and detached-eddy simulation (DES) models for indoor air flows and found that some RANS models showed good performance for simple cases but were not good for more complex flows such as those with a source of heat in the room, while LES was shown to be the most stable and accurate. Several studies used high-resolution CFD such as LES[32–37] and direct numerical simulations (DNS)[38–41] to investigate the dispersion of exhaled material from expiratory flows. Since DNS is the most computationally demanding, studies that employed this method have mostly investigated the details of the fluid dynamics of short expiratory events such as coughs,[38,41] or very short conversations,[40] and do not simulate the mid/long term development of flow patterns and particle dispersion at room scale. LES studies such as those by Vuorinen *et al.*[32] and Auvinen *et al.*[34] investigated particle dispersion in large spaces; however, both studies opted to use only two monodisperse particle size bins for aerosols.

CFD studies investigating particle dispersion in indoor spaces mostly use the Eulerian–Lagrangian (E–L) approach along with the RANS method (e.g., see Table I in Pallares and Fabregat[42]). In the E–L method, each individual particle is tracked separately and the motion is computed using Newton's second law. This approach allows for the detailed analysis of particle dispersion pattern and behavior based on particle diameter. In contrast, the Eulerian–Eulerian approach considers the particles as another continuum, and the relevant governing equations are solved to give information on the concentration field.[43] This method cannot track individual particles; therefore, it may be unsuitable when a polydisperse particle size distribution is used where the behavior based on particle diameter needs to be examined in more detail. Previous LES studies that used the E–L approach, used the particles as tracers,[33] included only small particles,[37] or when using a polydispersed particle size distribution, they do not look at dispersion at room scale.[35] While the LES study by Pendar and Páscoa[44] looked at room scale and used polydispersed particles, they did not consider the smallest aerosols (the minimum particle diameter in their study was 40 μm).

The effect of temperature on the spread of exhaled material has been investigated in the past both experimentally and numerically.[20,21,45–50] Usually, this is done in the context of modeling the effects of displacement ventilation (DV) on the dispersion of contaminants in indoor spaces. DV works on the principle of thermal stratification whereby cooler low velocity air is introduced near the floor level, spreads across it, and is entrained into the rising convective boundary layer flows generated near the heat sources,[51] creating a vertical temperature gradient. The entrained contaminants rise upwards and are extracted at the ceiling, creating a zone of clean air in the occupation region, while a contaminated zone is located near the ceiling.[52] It is known that a vertical temperature gradient can lead to the lock-up phenomenon whereby contaminants become trapped below the warmer contaminated ceiling level.[52] The strength of the temperature gradient determines the lock-up height; therefore, it is an important factor for infection risk considerations in indoor spaces with DV. Liu *et al.*[46] investigated experimentally the effect of thermal stratification on expiratory particle dispersion in a water tank, using three different sizes of glass bead particles to represent small, medium, and large expiratory particles. They found that the largest particles are unaffected by thermal stratification, while the smallest particles follow the flow passively and their upward movement is trapped by thermal stratification, leading to their horizontal reach being extended. The experimental studies by Lai and Wong[49,50] on aerosol transport in a scaled chamber with thermal manikins also showed that compared to mixing ventilation, thermal stratification leads to a higher concentration of particles in the breathing zone. Nielsen *et al.*[45] studied experimentally the influence of a temperature gradient in DV on the risk of infection between two individuals, using a tracer gas to represent the exhaled material. Their work also showed the lock-up effect and trapping of exhaled material, demonstrating that there is a significant increase in direct exposure to exhaled contaminants compared to a fully mixed case, in particular when the distance between the source and susceptible individuals is less than 80 cm.

Numerical studies investigating the effect of temperature on the dispersion of exhaled material have mostly used RANS. Foat *et al.*[20] looked at the effect of isothermal temperatures of 16, 20, and 28 °C and found no clear correlation between temperature and exposure to the exhaled material; however, the study did not consider thermal stratification effects (the thermal plume from the manikin used in the study did not have considerable effect due to the strength of the mechanical ventilation). Pei *et al.*[47] used Eulerian–Eulerian RANS to investigate the effect of ventilation strategies on the transport of 1 and 10 μm aerosol particles between two seated thermal manikins and found that thermal stratification effects in DV increase the distance these particles can travel. An increase in exposure to exhaled material in the breathing zone within the 2 m physical distance was also observed when compared to mixing ventilation. Furthermore, the study showed that the exhalation jet produced during speaking can penetrate the thermal plume of the susceptible individual. This study did not use a polydispersed particle size distribution; therefore, the combined effect of temperature gradient and particle sizes was not

investigated. The study by Liu *et al.*[21] included some numerical modeling of displacement ventilation effects, but it was not the primary focus of their work and only 100 μm particles or tracer gas was used in their DV simulations. Liu *et al.*[48] applied Eulerian–Lagrangian LES to study the role of airflow on aerosol transport that led to a COVID-19 outbreak in a restaurant in Guangzhou, China. They simulated heat effects from the food on the table and human bodies and used their results to produce a spatial risk of infection with good agreement in regard to the reported infections. The aerosols used in their study were based on data from Shao *et al.*;[24] therefore, a majority of the particles were 5 $<\mu$ m. Li *et al.*[9] also simulated airflows in the same restaurant with 5 μm sized particles using RANS, with their findings supporting the role of inadequate ventilation in airborne transmission of SARS-CoV-2.

In the studies mentioned above (experimental and numerical), thermal stratification was introduced either via thermal manikins or other heat sources. That is, the effects were "local" and did not respond to preexisting stratification throughout the room. Furthermore, the tracking of polydispersed particles experimentally at room scale is challenging, while numerical studies often simplify particle size distributions that may not necessarily be representative of the particle size distributions emitted from humans during expiratory activities. This may lead to assumptions being made *a priori* about which particles may be important. To the best of our knowledge, there are no current studies that have investigated thermal stratification effects whereby a vertical temperature gradient is imposed throughout the whole domain to study its effect on the exhalation jet and the polydispersed particles suspended within it at room scale. The question of whether vertical temperature gradients acceptable from thermal comfort perspective (e.g., see Möhlenkamp *et al.*[53]) are acceptable from a cross-infection point of view remains to be explored.

In this paper, we use an in-house Eulerian–Lagrangian LES solver to investigate the effect of thermal stratification on the transport of polydispersed expiratory particles emitted during speaking at room scale. We analyze the effect of increasing temperature gradient within what is acceptable from a thermal comfort perspective and compare the results to an isothermal case at a room temperature of 20 °C. Furthermore, the effect of room size is investigated by running the same set of simulations on a smaller domain. We compute the spatiotemporal evolution of particle volume fraction to quantify the effect of thermal stratification on the reach of different particle size categories within the room. The evolution in the time of aerosol concentration within the breathing zone is also quantified. The aim of this work is to investigate to what extent thermal stratification affects airborne cross-infection and which temperature gradient leads to lock-up of particles at the breathing height. Furthermore, we aim to study the impact of thermal stratification on different sized particles under realistic expiratory conditions at room scale.

This paper is organized as follows. The governing equations for the continuous and dispersed phases and details of simulation setup are presented in Sec. II. The mesh sensitivity analysis and validation are presented in Secs. III and IV. The results and discussion are presented in Sec. V, and concluding remarks are provided in Sec. VI.

II. GOVERNING EQUATIONS AND NUMERICAL FRAMEWORK

An expiratory event is a multiphase flow problem composed of a turbulent buoyant jet release (the carrier phase) in which particles of various sizes are suspended (the dispersed phase). In the present work, a finite-difference Eulerian–Lagrangian point-particle large-eddy simulation in-house code MultiFlow3D is used to solve the equations of 3D fluid motion.[54–59] The continuous phase (air, reference $\rho = 1.2\,\mathrm{kg/m^3}$) is modeled in a Eulerian framework on a staggered grid, while the dispersed phase (liquid particles, $\rho_p = 1000\,\mathrm{kg/m^3}$) is resolved by a Lagrangian particle tracking algorithm[54] where the spatiotemporal tracking of every particle is performed.

A. Continuous phase

The airflow is governed by the incompressible three-dimensional space-filtered mass, momentum, and energy conservation equations. Using Einstein notation,

$$\frac{\partial u_j}{\partial x_j} = 0, \tag{1}$$

$$\frac{\partial u_i}{\partial t} + \frac{\partial u_i u_j}{\partial x_j} = -\frac{1}{\rho_{ref}}\frac{\partial p}{\partial x_j} + 2\nu\frac{\partial (S_{ij})}{\partial x_j} - \frac{\partial \tau_{ij}}{\partial x_j} + \xi_i + S_b + S_m + S_{IBM}, \tag{2}$$

$$\frac{\partial T}{\partial t} + u_j\frac{\partial T}{\partial x_j} = \alpha\frac{\partial^2 T}{\partial x_j \partial x_j} + S_T, \tag{3}$$

for $i = 1, 2, 3$, where u_i is the velocity component in the i direction, ρ_{ref} is the reference density, p is pressure, t is time, ν is the kinematic viscosity $= 1.51 \times 10^{-5}$ m^2/s, S_{ij} is the strain rate tensor, and ξ_i is the contribution of the particles to the flow of air. The unresolved turbulence is accounted for by the Reynolds stress tensor term, τ_{ij}, where the Smagorinsky sub-grid scale model is used to calculate it, with Smagorinsky constant set to 0.1. The source term S_b accounts for the buoyancy effects (acting in the vertical $i = 3$ direction) produced by the relatively small differences in the fluid's density due to changes in temperature using the Boussinesq approximation, with $S_b = \beta g(T_i - T_o)$, where β is the coefficient of thermal expansion set to 0.003 47 K^{-1}, g is the gravity acceleration vector, T_i is the instantaneous temperature at any point in the 3D space, and T_o is the reference temperature set to 20 °C. The source term S_m represents the momentum produced by the breath, which is defined as the breath flow rate divided by the mouth's area. The source term S_{IBM} represents the force distribution function used in the immersed boundary method, which was used for simulating the fluid–solid interaction between the human body and the continuous phase. More detail on this can be found in Peskin.[60] The term α in Eq. (3) represents the thermal diffusivity, while S_T represents the source term for the temperature at the mouth. Second-order central differencing schemes are used for discretization of both the diffusive and convective terms in the equations presented above, while a two-step Runge–Kutta algorithm is used for time discretization. The code is based on a predictor–corrector fractional step method with the solution of the Poisson pressure equation using a multi-grid method as the corrector.

B. Dispersed phase

The movement of expiratory particles is simulated using a Lagrangian particle tracking algorithm,[54] where each particle is represented by a volumeless Lagrangian point that is tracked in space and time. Interaction between particles as well as evaporation and humidity effects are not considered in the present study. The latter imply that our particles will not vary in size, which will allow us to isolate the effect of thermal stratification on expiratory particles depending on

their size, irrespective of other environmental conditions. On the assumption that the particles are rigid and spherical, their motion is represented by Newton's second law as follows:

$$m_p \frac{\partial u_{p,i}}{\partial t} = F_{p,i}, \tag{4}$$

where m_p and $u_{p,i}$ are the particle mass and particle velocity component in the i direction, respectively. $F_{p,i}$ is the sum of the interfacial forces acting on the particle in the i direction with the following forces considered:[61]

$$F_{p,i} = F_{G,i} + F_{S,i} + F_{A,i} + F_{D,i} + F_{L,i}, \tag{5}$$

where $F_{G,i}, F_{S,i}, F_{A,i}, F_{D,i}, F_{L,i}$ are the gravity/buoyancy, fluid stress, added mass, drag, and lift forces, respectively, acting on the particle in the i direction and are approximated by semi-empirical formulas. Note that $F_{G,i}$ acts in the vertical direction only (i.e., $i = 3$). Details of the individual formulations for each of the forces can be found in Fraga *et al.*[54] and are not repeated here for brevity. The general equation representing the motion of particles is given by

$$\frac{\partial u_{p,i}}{\partial t} = -\frac{1-\gamma_p}{\gamma_p + C_A} g + \frac{1+C_A}{\gamma_p + C_A}\frac{Du_i}{Dt} + \frac{3}{4}\frac{C_D}{d_p(\gamma_p + C_A)}|u_{p,i} - u_i|(u_{p,i} - u_i) - \frac{C_L}{\gamma_p + C_A}(u_{p,i} - u_i) \times \omega_i, \tag{6}$$

where C_A is an empirical coefficient set to 0.5 for a sphere,[61] g is the acceleration due to gravity, u_i is the fluid velocity (i.e., air in this case) at the particle's geometric center location, $(u_{p,i} - u_i)$ is the slip velocity (i.e., the difference between the particle and air velocity), d_p is the particle diameter, ω_i is the fluid vorticity, and $C_L = 0.53$ is the lift coefficient for a sphere. The density ratio between the two phases is represented by $\gamma_p = \rho_p/\rho$, where the particle density, ρ_p, has a constant value, while the air density, ρ, varies linearly with air temperature. Note that this is a general equation, and the first term of Eq. (6) is only present in the $i = 3$ direction calculation. C_D is the drag coefficient dependent on the local Reynolds number and is calculated from the standard drag curve as follows:[62]

$$C_D = \begin{cases} 24/Re_p & \text{for } Re_p < 1, \\ (24/Re_p)\left(1 + 0.5Re_p^{0.687}\right) & \text{for } 1 \le Re_p \le 800, \\ 0.44 & \text{for } Re_p > 800. \end{cases} \tag{7}$$

From the Stokes number calculation, $St = \rho_p d_p^2/18\mu\tau_F$, where τ_F is some time characteristic of the flow[63] and is taken as 0.1 s during speech,[33] and $St \sim 3 \times 10^{-3}$ and 3×10^{-5} for a 10 and 1 μm particle, respectively. Therefore, based on the St calculations, particles with $d_p < 10\ \mu m$ are treated as passive in the present simulations [i.e., Eq. (6) is used to calculate the particle velocity when $d_p \ge 10\ \mu m$, while particles with d_p smaller than this are assigned the Eulerian velocity at that particle location]. The above equations of motion for the expiratory particles are solved using a two-way coupling approach, whereby the particles interact back and forth with the surrounding flow field. The accumulated particle volume fraction, ϕ_p, in a given computational cell is computed in each time step to track the path of the particles and the evolution of their concentration throughout the domain as follows:

$$\phi_p = \phi_p^{t-1} + \sum_{\forall n \in cell} \frac{V_{p_n}}{V_{cell}}, \tag{8}$$

where ϕ_p is the current time step particle volume fraction, ϕ_p^{t-1} is the previous time step particle volume fraction, V_{p_n} is the volume of the particle n in the cell, and V_{cell} is the volume of the computational cell. Based on the analysis of particle motion in a test run, separate fractions $\phi_{p,small}$, $\phi_{p,medium}$, $\phi_{p,large}$ were also computed. The smallest particles remain airborne much longer than larger particles and follow a different trajectory; therefore, to track and visualize only their path more clearly, the following intervals were considered separately:

$$\phi_{p,small}: 1 \le d_p \le 20\ \mu\text{m},$$
$$\phi_{p,medium}: 20 < d_p \le 87.5\ \mu\text{m},$$
$$\phi_{p,large}: 87.5 < d_p \le 375\ \mu\text{m}.$$

C. Particle size distribution and breath cycle

The particle size distribution was adapted from Duguid[64] to match a particle count of 195 particles/second[65] as shown in Fig. 1. In Duguid's[64] work, the particles were classified within size intervals; in the present simulations, the class mark of each interval is used as the particle diameter assigned to a specific particle count. The particles are released in the horizontal direction at a rate of 195 per second from the subject's mouth along with the exhalation jet from a height z = 1.7 m, and once they reach the limits of the domain, they are removed. The mouth is modeled as a 1.34 cm wide square, giving a 1.8 cm^2 mouth area,[66] and the particles are initially distributed randomly across this area. Since a majority of the exhalation comes from the mouth during speaking,[66] this is the most significant source of momentum; therefore, the nasal jet is not considered in the present work. Based on Abkarian *et al.*,[33] one breath cycle is assumed to last for 5 s, with 4 s spent exhaling continuously and 1 s inhaling—during the 1 s inhalation period, the release of particles and the exhalation jet are paused. This breathing cycle repeats throughout the whole simulation time. The exhalation flow rate and temperature used in all cases are 0.5 l/s and 34 °C, respectively.[33,67]

D. Computational domain

Figure 2 shows the domain setup where an infected individual is speaking for 180 s—the exhalation jet and particles are released into an undisturbed environment. A uniform computational grid is used in all

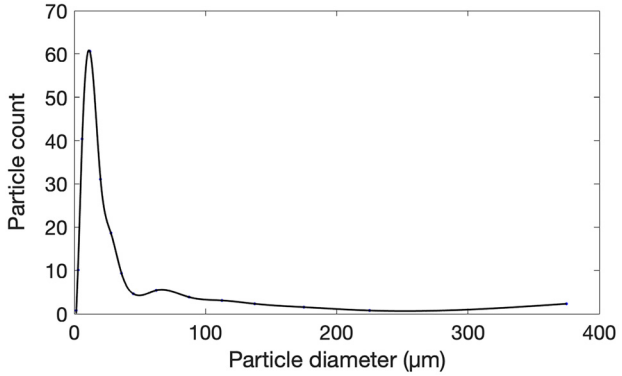

FIG. 1. Particle size distribution during speaking used in the simulations.

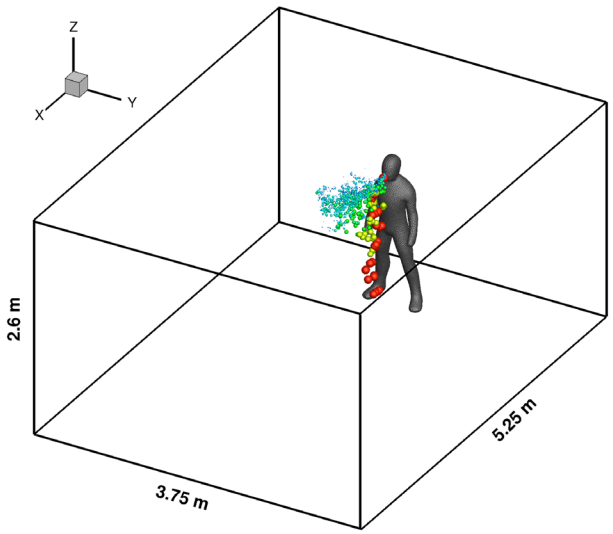

FIG. 2. Isometric view of the domain setup for large room cases and the position of the infectious individual.

cases, with time step dt = 0.0005 s. Three different grid resolutions were tested. The immersed boundary method[60] was used to represent the body, which is composed of Lagrangian markers defining its surface where a no-slip boundary condition is imposed. The effect of the body thermal plume was not considered in the present work. Six cases in total are presented, investigating the effect of temperature gradients and room size on particle dispersion as described in Table I where case letters S and L denote the small and large room geometries, respectively, and the number after the letter indicates the value of the temperature gradient. As with any transient turbulent flow, if these experiments were performed physically, each realization would produce a slightly different result due to the chaotic nature of turbulence; in our computational setup, we have complete control over the exact initial conditions; hence, our deterministic model will produce a unique solution that should be understood as the ensemble-average of all the physical tests with slightly different initial conditions. Regardless, our analysis is not based on the fate of an individual particle but the collective and consistent behavior of thousands of particles across the flow field.

When the temperate gradient dT/dz is set to 0, a uniform room temperature of 20 °C is adopted. When thermal stratification is considered, a linear increase in the room temperature with height is implemented. There are two relative stratification strengths: the weaker case considers a temperature of 20 °C at the floor that increases at a rate of 1 K per meter, while the stronger case elevates the gradient to 2 K/m. The boundary conditions for all walls are set to no-slip. Note that particles in all figures are scaled up for visual purposes only and do not represent the "true" particle size in relation to the domain.

TABLE I. Case details.

Case[a]	dT/dz (K/m)	Room size (L × W × H) in m
S0	0	
S1	1	3.5 × 2.5 × 2.6
S2	2	
L0	0	
L1	1	5.25 × 3.75 × 2.6
L2	2	

[a]S = small room, L = large room.

III. MESH SENSITIVITY ANALYSIS

A major challenge simulating dispersed flows is to reach a level of discretization that is compatible with the larger computational domain while capturing the individual motion at the particle scale. In the current case, the difference in characteristic scales between the continuous and dispersed phases is so extreme that we assume that all particle-scale motion is subgrid. The ability of the chosen grid resolution to capture the relevant flow features adequately is investigated by testing 3 different uniform mesh resolutions for the L0 base case. The mesh resolution is doubled each time with the fine, medium, and coarse mesh sizes being equal to 6.25, 12.5, and 25 mm, respectively. The sensitivity parameters are the average streamwise velocity and temperature and the accumulated small particle volume fraction. Figure 3 shows the jet profile color-coded by the average streamwise velocity for the different mesh resolutions. The slice is located in the middle of the Y plane, and the effect of the jet profile on particle dispersion can

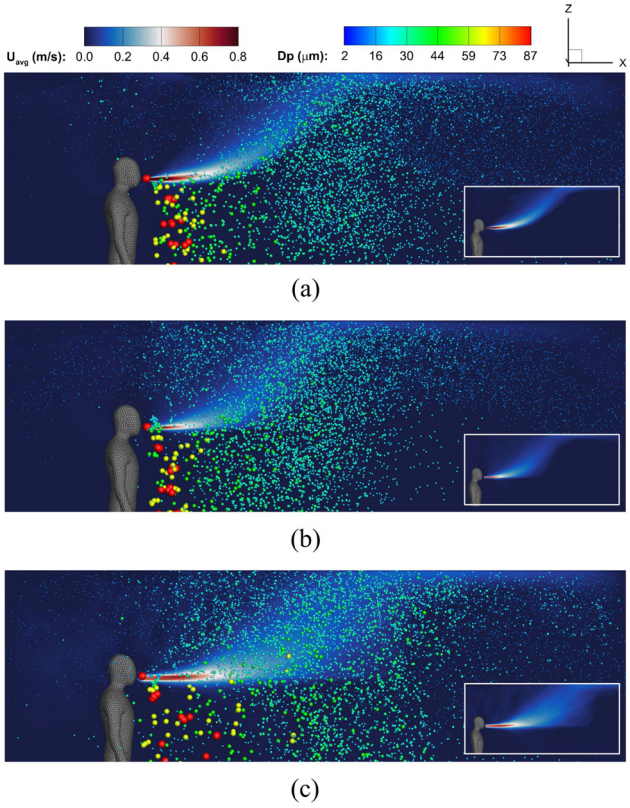

FIG. 3. Jet profile color-coded by time-averaged streamwise velocity, and particle dispersion after 180 s for (a) fine, (b) medium, and (c) coarse mesh resolutions for L0.

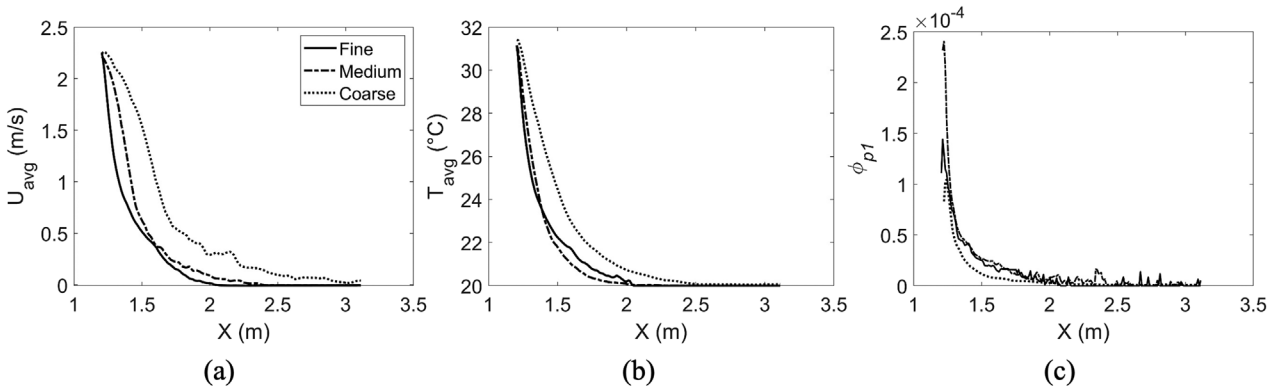

FIG. 4. Horizontal profiles extracted within the center of the breathing jet of (a) average streamwise velocity, (b) average temperature, and (c) small particle volume fraction for different mesh resolutions using L0 case.

be seen by the instantaneous particle distribution at t = 180 s. The shape of the breathing jet is much wider in the coarse mesh [Fig. 3(c)] than in the fine and medium meshes [Figs. 3(a) and 3(b), respectively]. Furthermore, the curvature of the exhalation jet is less clearly defined and occurs further downstream compared to Figs. 3(a) and 3(b). All particles are overdispersed as a result in the coarse mesh resolution. Figure 4 shows the variation of the three sensitivity parameters in the streamwise direction, starting at the breathing jet release point (x = 1.2 m). Given the mouth's size compared to the total volume of the room, the near-field of the jet at the mouth is under-resolved, particularly for the medium and coarse meshes. This is a necessary compromise given the computational requirements of these simulations, acceptable as long as they do not compromise the momentum and energy inputs at the release points.[32] The first ∼1.5 m from the point of release defines two regions: (1) inertia dominated and (2) buoyancy dominated. This region is crucial to capture the general path of the jet, which affects particle dispersion. The results in Fig. 4 show that both the fine and medium mesh resolutions produce similar results, while the coarse mesh overpredicts the average streamwise velocity and temperature. This can be attributed to an excess of dissipation induced by the SGS model on energy-containing scales due to the low mesh resolution. This will result in an underprediction of the turbulent kinetic energy, leading to overprediction of the kinetic energy; hence, the higher mean flow is seen in Fig. 4(a). As the coarse mesh overpredicts the average streamwise velocity and temperature, it leads to the underprediction of $\phi_{p,small}$. This is because as the breathing jet becomes overdispersed, the small particles suspended within it follow its path as seen in Fig. 3(c). Based on Figs. 3 and 4, the coarse mesh is insufficient to capture the relevant scales of the exhaled jet, while the fine and medium mesh resolutions show convergence. Based on this, the medium mesh resolution (12.5 mm) is chosen as it provides very similar results to the fine mesh while being computationally less intensive.

IV. MODEL VALIDATION

The numerical model's ability to correctly predict the exhalation jet's trajectory is compared against the model developed by Zhou *et al.*,[68] which has been validated against the results from full-scale experiments carried out by Qian *et al.*[69] The non-dimensional theoretical buoyant jet dispersion model considers the centerline trajectory of a buoyant jet released continuously into a thermally uniform and thermally stratified environment. The computational domains are 2 × 1.5 × 3 m for the isothermal case and 5 × 1.5 × 1.2 m for the stratified run; in both cases, the domain was chosen to be sufficiently large to ensure that none of the walls affect the jet trajectory and impact the results. The mesh resolution and inlet shape replicate those of the principal room simulations with particles. For the thermally stratified cases, the vertical temperature gradient was considered to be linear, while in the thermally uniform cases, the ambient air temperature was set to 21 °C. The exhaled air in all cases was at 34 °C. The ambient air in all cases was treated as still, and no other sources of heat apart from the exhalation jet were considered so that only the trajectory of the exhaled flow could be studied. Cases 15 (temperature gradient, dT/dz = 2 °C/m) and 6 (uniform temperature) from Zhou *et al.*[68] were replicated in our numerical simulations, which ran for 120 s and are shown in Figs. 5 and 6, respectively. A passive tracer entrained in the jet is used to visualize its trajectory and compare it to predictions by Zhou *et al.*[68] The slice in the numerical simulations is shown in the middle of the Y plane and is

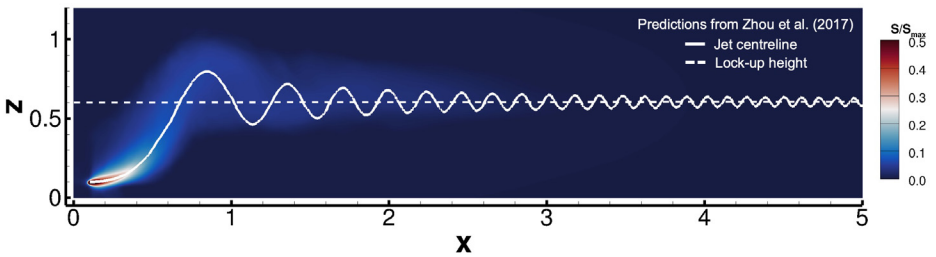

FIG. 5. Comparison of the jet's trajectory in numerical simulations with the predicted jet centerline trajectory from Zhou *et al.*[68] (solid white line) for case 15. The lock-up height from the theoretical model is marked by the dashed line.

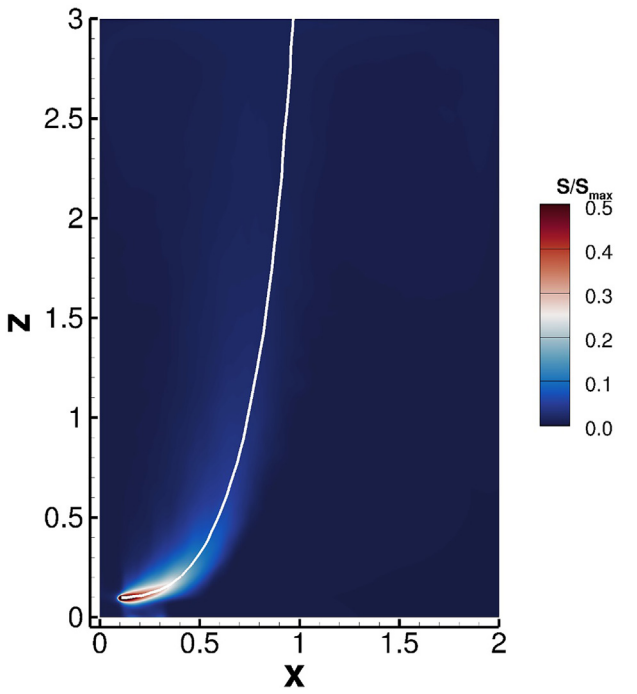

FIG. 6. Comparison of the jet's trajectory in numerical simulations with the predicted jet centerline trajectory from Zhou *et al.*[68] (solid white line) for case 6.

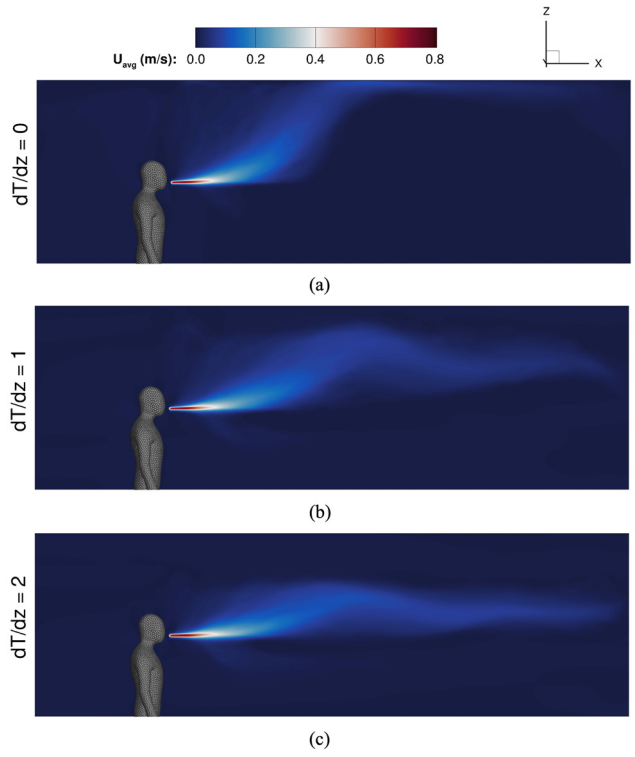

FIG. 7. Comparison of breathing jet behavior released into ambient air subjected to increasing temperature gradient colored by the time-averaged streamwise velocity.

colored by the time-averaged normalized passive tracer S/S_{max}, where S_{max} is the maximum value of S.

In both cases, the jet's trajectory visualized by the passive tracer shows a good agreement with the centerline predictions by the theoretical model presented in Zhou *et al.*[68] The thermal length, l_m, is the point at which the jet trajectory will curve upwards, and Zhou *et al.*[68] calculated l_m to be 0.2 m for cases 6 and 15. Figures 5 and 6 show that our numerical model predicts this well, as the jet's curvature in both numerical simulations also occurs 0.2 m away from the point of release. In the stratified case, the oscillating trajectory and the lock-up height predicted by Zhou *et al.*[68] fall within the bounds of the oscillating passive tracer contour. This shows that our model can predict well the buoyancy effects associated with the release of warm exhaled air into both thermally uniform and thermally stratified ambient air.

V. RESULTS AND DISCUSSION

A. Exhalation jet behavior

During any expiratory activity, the released exhalation jet will be buoyant due to its warmer temperature (34 °C in present cases) compared to ambient room air. Figure 7 shows how the varying temperature gradient of ambient air affects the trajectory of this exhalation jet, visualized by the average streamwise velocity for L cases. In all 3 cases, there is an inertia-dominated region where the jet moves forward in the streamwise direction due to its momentum, before an upward curvature is seen at the point where the buoyancy and average momentum of the jet become comparable, in agreement with the observations by Bourouiba *et al.*[1] In our cases, this point is found approximately 80 cm from the speaker. The effect of thermal stratification on the jet's trajectory becomes apparent once it begins to curve upwards.

When the jet is released into a uniform temperature environment [Fig. 7(a)], there is a high net temperature difference with the ambient air. Past the inflection point, the jet will continue to rise rapidly upwards as the buoyancy effects are strong—the rising effect will be arrested by the ceiling or in the case of a very high ceiling environment until the temperature of the jet and ambient air become comparable. In a thermally stratified environment, the net temperature difference between the jet and ambient air will be slightly lower. Past the inflection point, the jet will rise up to some maximum height (~2.4 m for L1 and 2.2 m for L2, respectively) before coming back down and oscillating about the lock-up height [~2.1 m for L1 and 1.9 m for L2 as seen in Figs. 7(b) and 7(c), respectively]. This is due to the air entrained in the jet dispersing and cooling down to a similar temperature to that of the surrounding ambient air, at which point it will start to float back down, trying to reach equilibrium and leading to the oscillations seen in Figs. 7(b) and 7(c) as the process repeats. The behavior of the jet is consistent with predictions by Liu *et al.*[70] and experimental studies by Liu *et al.*[46]

Based on the exhalation jet trajectory, the following conclusions can be drawn: (1) thermal stratification has no effect on the jet's trajectory in the very near-field zone of the infectious individual (approximately first 80 cm for the conditions presented here) as momentum dominates in this zone; (2) the lock-up height gets closer to the breathing height as ambient air temperature gradient increases, and the

oscillations of the jet become less defined; (3) thermal stratification effects become important once the jet begins to curve upwards as buoyancy effects start to dominate; and (4) the point at which the jet bends upwards in all 3 cases occurs at approximately the same point; therefore, it can be inferred that it depends on the jet's initial momentum. Increasing thermal stratification overall does not affect the point at which the curvature of the jet begins but only the rate of this curvature, i.e., how far and steeply this jet will initially travel upwards. It should be noted that the exhaled jet temperature varies from person to person;[67] therefore, the jet trajectory in the buoyancy dominated region described in this section may vary to some extent, with the initial jet temperature being slightly higher or lower than the 34 °C used in this study.[67]

B. Particle transport and suspension within the exhalation jet

Figure 8 shows the instantaneous streamwise velocity field within the half-width plane at t = 180 s for cases L0 (a), L1 (b), and L2 (c). The exhalation jet entrains particles ranging from 1.5 to 375 μm, and for clarity and visual purposes, particles larger than 100 μm are not shown. To better visualize the effect of thermal stratification on aerosol lock-up, a focused view emphasizing the distribution of smaller particles ($d_p < 30$ μm) is presented on the right column. The smallest particles (dark blue) remain suspended in the jet and reach all the way to the end of the room, showing that long range aerosol transmission is possible in all three cases. In the isothermal case L0, most of them remain just above the breathing zone at a height of ≥ 2 m as they are carried upwards by the buoyant exhalation jet and accumulate near the ceiling. They reenter the breathing zone only when the jet reaches the end of the room and begins a recirculating pattern, dragging the smallest aerosols with it. In contrast, in the presence of stratification [Figs. 8(b) and 8(c)], the smallest aerosols no longer accumulate by the ceiling and instead are found closer to the breathing zone as the temperature gradient is increased. While 12 μm particles in L0 case stay airborne along with the smallest aerosols, in cases L1 and L2 a large portion of these particles detach from the jet and accumulate around the z = 1.6 and z = 1.5 m heights, respectively, just below the breathing zone as shown in the focused view of Figs. 8(b) and 8(c). This indicates that thermal stratification can trap aerosols at different heights depending on their diameter up to some size threshold. Our results show that the threshold exists between the 12 and 20 μm aerosol size interval whereby their behavior changes from locked-up by stratification to a continuous fallout from the jet.

There is a notable difference in the reach of the medium aerosols ($d_p \approx$ 20–30 μm, light blue) between L0 [Fig. 8(a)] and L1 and L2 cases [Figs. 8(b) and 8(c)], whereby thermal stratification extends their reach by almost a further meter compared to L0 case. This is due to the stratification limiting the upward movement of the exhalation jet, forcing it to continue propagating forward, driven by cyclic turbulent puffs. In all three cases, these particles initially remain suspended within the jet before they begin to fall out continuously; hence, their presence along most of the room height is shown in Fig. 8. In the thermally stratified cases, particularly L1, the downward jet oscillation [at x ≈ 3.2 m mark in Fig. 8(b)] drags these particles down and not as many are present in the subsequent upward oscillation. These medium aerosols are too "heavy" in comparison to the dark blue aerosols to be re-entrained into the jet once they have detached; hence, in both stratified cases, we see that the majority of the 20–30 μm particles reach a distance that coincides with the end of the first downward oscillation ($x \approx 3.8$ m). After this point, only some particles in this size range remain in the jet and are able to travel a further meter. In the isothermal case L0, the reach of medium aerosols coincides with the point at which the jet's trajectory is arrested by the ceiling. The velocity reduces slightly as the jet adjusts its path, so the bulk of the suspended particles reaches the x ≈3 m point. Like in the stratified cases, some particles do remain suspended past this point and are also able to travel a further meter.

The larger aerosols ($d_p \approx$ 30–45 μm, green) are carried up to a maximum distance of approximately 1.4 m away from the infectious person. In the thermally stratified cases, the majority of these particles are concentrated near the x ≈ 1.8–2 m mark (i.e., 0.6–0.8 m away from the speaker). For L0 [Fig. 8(a)], these larger aerosols are not concentrated around a particular horizontal distance from the speaker and a more continuous detachment from the upward moving jet is observed. The droplets (yellow and red) in all cases are too heavy and fall out very quickly from the jet, reaching only 20–50 cm away from the speaker. This behavior is consistent with findings by Cortellessa *et al.*[8] who showed that large droplets only contribute to the risk of infection at distances well below 0.6 m from a speaking person. One of our key findings is that droplets do not follow a ballistic trajectory.

The main conclusions drawn here are: (1) thermal stratification constrains the upward movement of the exhaled material, with this effect becoming stronger as temperature gradient increases; (2) stratification increases the horizontal reach of medium aerosols ($d_p \approx$ 20–30 μm) and leads to an increased concentration of smaller aerosols closer to the breathing height; (3) larger particles ($d_p > 60\mu m$) are unaffected by stratification effects, do not follow a ballistic trajectory, and fall out within 0.5 m of the infected individual; (4) small aerosols ($d_p < 20\mu m$) can travel up to 4 m away from the infectious source for the given conditions presented in our simulations; and (5) aerosols up to 12–20 μm can be locked-up at different heights by thermal stratification—beyond this size, they continuously fall out of the jet. Since particle evaporation or growth is not included in the present work, the particle size distribution does not change with time. One major purpose of this work is to simulate the impact of particle size on their spread under different conditions. Keeping their size constant provides a more clear picture of the different particle behaviors, allowing us to group them without *a priori* assumptions. Including evaporation would not affect how far a particle of a given size may travel, yet it affects the *number* of particles of that size that we see over time. For example, had evaporation effects been included and assuming a low humidity scenario, some larger aerosols may have evaporated down to a size small enough that would allow them to stay airborne for longer.

C. Particle dispersion pattern

Figure 9 shows 3D and top-down views of the instantaneous particle dispersion for all six cases at t = 180 s. The majority of the dispersion is parallel to the exhalation jet as ventilation effects are not considered in the present work. Particle transport is driven by the exhalation jet and buoyancy as there are no other sources of air movement. Room size does not have a critical impact on aerosol dispersion patterns, besides constraining them. Large room simulations exhibit very clearly the lock-up of the smallest fractions discussed in Fig. 8. This is not as evident in the small room cases as the jet hits the wall at

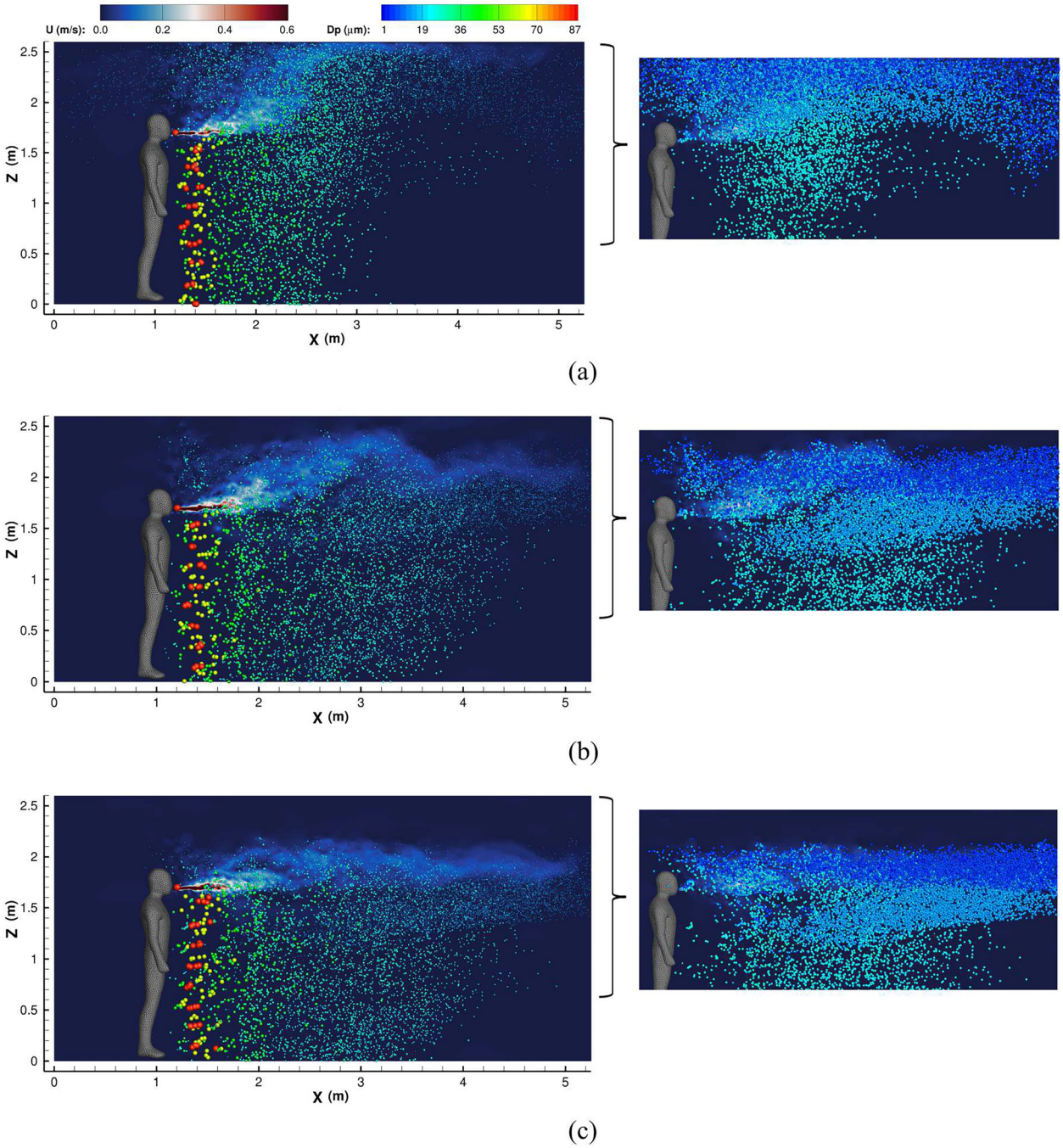

FIG. 8. Influence of thermal stratification on particle dispersion at 180 s for (a) L0, (b) L1, and (c) L2. The continuous phase is color-coded by the instantaneous streamwise velocity; particles are colored by size. Right column: focused view of particles $<30\,\mu$ m.

a closer distance from the point of release. The recirculation leads to a bigger dispersion of the smallest particles throughout as the airflow returns toward the speaking person. The recirculation becomes more pronounced with increasing stratification, as can be appreciated in the top-down view for cases S1 and S2. Recirculation in the larger room cases also occurs, yet is weaker in comparison to the small room cases since the velocity of the jet would have decayed along a longer distance from the speaker before impacting the wall. The top-down figures for all six cases illustrate a clear difference in the dispersion pattern between thermally stratified and isothermal cases. In L0 and S0 cases,

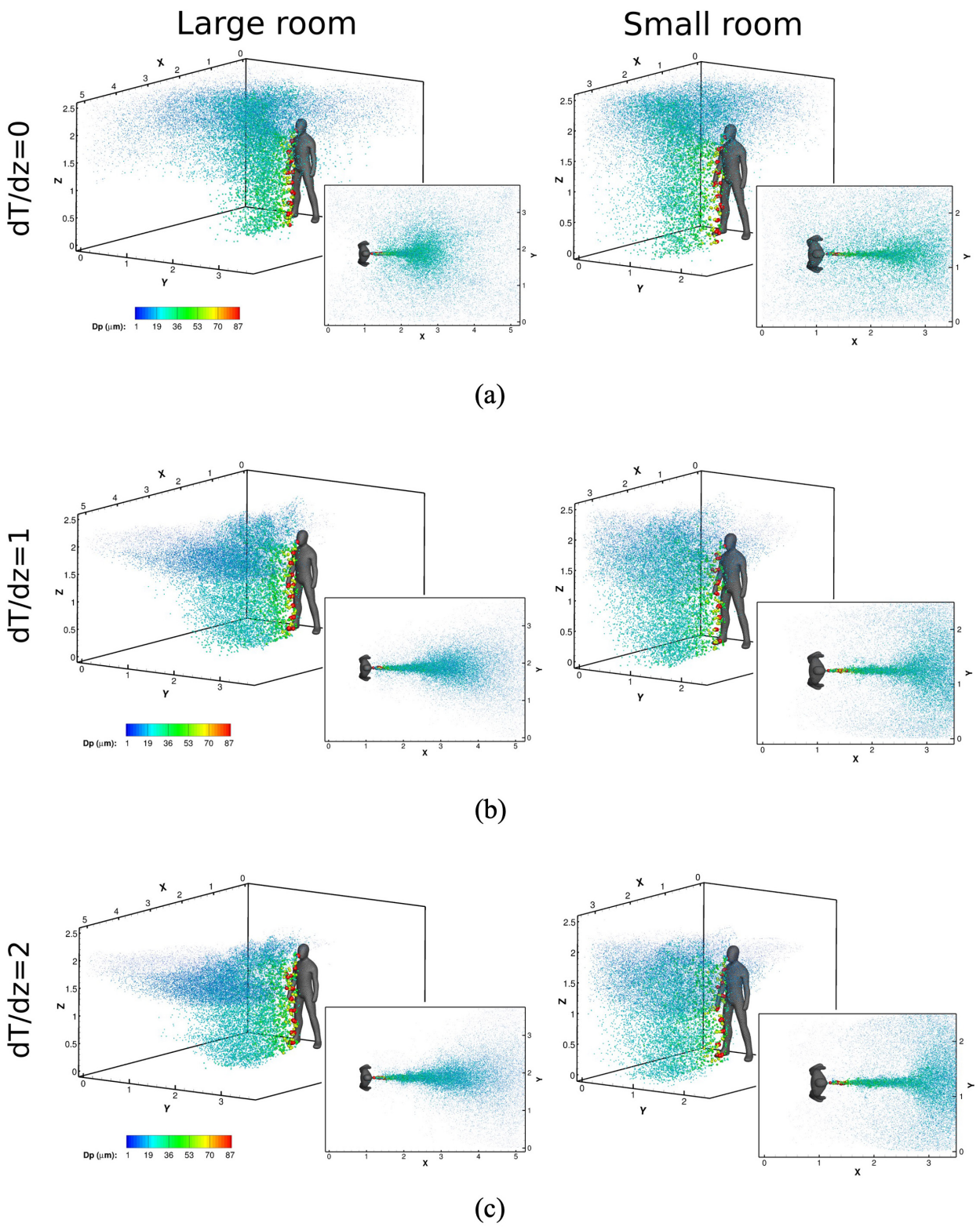

FIG. 9. Instantaneous particle dispersion at 180 s for large room (left) and small room (right) at temperature gradients (a) 0, (b)1, and (c) 2 K/m.

since the jet continues rising upwards due to its buoyancy, it reaches the ceiling and spreads out across it. In cases with thermal stratification, the particles are concentrated around the centerline of the exhalation jet before they spread out laterally as the jet decays to its surroundings.

For the stratified cases shown in Figs. 9(b) and 9(c), when the room size/geometry does not heavily influence the exhalation jet flow, the dispersion pattern takes a cone-like appearance that becomes wider as the distance from the speaker increases. This is due to buoyancy effects: closer to the source, the temperature and velocity of the jet are higher as little ambient air has been entrained into it; therefore, the particles travel forward with it. As the jet continues moving forward, it entrains more ambient air and its temperature and buoyancy reduce, and its velocity decays to the surroundings. This leads to the lateral spreading of the jet and the smallest particles suspended within it as the distance from the speaker increases.

The main conclusions drawn here are that (1) a smaller room constrains the flow structures and enhances recirculation, bringing more particles back toward the subject; (2) the enhanced recirculation breaks to an extent the stratification layers in small rooms; and (3) as the temperature gradient increases, expiratory particles follow the jet centerline more closely before they disperse laterally. Based on these results, to reduce the risk of infection during a face to face conversation where masks are not worn, a person should stand to the side of the speaker to avoid inhaling the highest concentration of aerosols.

D. Concentration of aerosols in the near-field breathing zone

Figure 10 defines the two zones proposed to quantify the effect of thermal stratification on the evolution over time of aerosol concentration $\phi_{p,small}$ in the breathing zone. Each zone covers a 1.575 × 1.25 m^2 area in the horizontal XY plane and has a height of 0.325 m. Volume fractions representing larger particles are not shown here since the focus is on particles that are trapped in the exhaled jet.

Figure 11 shows the integral values of $\phi_{p,small}$ in the breathing and upper zones for L0, L1, and L2 cases over 180 s. In the breathing zone [Fig. 11(a)], the small aerosol concentration is the same in all three cases during the first 15 s as the exhalation process is established and particles accumulate. Beyond this point, the concentrations diverge, with L2 case showing the steepest and highest growth, followed by L1 and L0. This was expected, as the higher ambient air

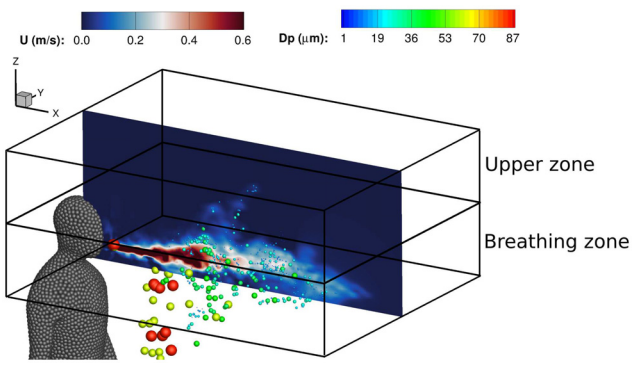

FIG. 10. Layout of the zones under consideration for aerosol build-up analysis.

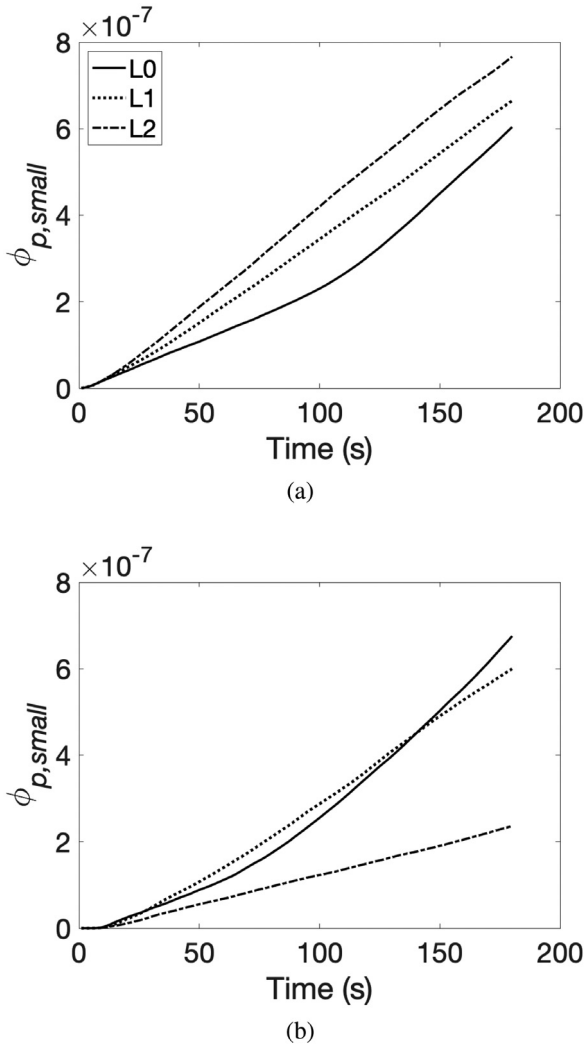

FIG. 11. Evolution over time of the small aerosol volume fraction ($1 \leq d_p \leq 20\ \mu$m) for (a) breathing zone and (b) upper zone as shown in Fig. 10 for L0, L1, and L2.

temperature gradient arrests the exhalation jet's upward trajectory, making it move forward within the breathing zone instead. In contrast, the jet in L0 continues its upward trajectory into the "upper zone," entraining the aerosols. At t = 180 s, the concentration of smallest aerosols in the breathing zone has increased by 10% and 27% for cases L1 and L2, respectively, in comparison with L0.

In the "upper" zone [Fig. 11(b), z = 1.95–2.275 m], the concentration of smallest aerosols is significantly lower in case L2 compared to that in L0 and L1 cases. This is due to the forward movement of the jet in a relatively "straight" line described earlier for the stratified cases (e.g., see Fig. 8). At 180 s, the concentration of smallest aerosols in the upper zone relative to case L0 is up to 12% and 65% lower for cases L1 and L2, respectively. High aerosol concentrations are present in this zone for both cases L0 and L1 since the lock-up height of L1 was ~2.1 m as identified in Sec. V A. An interesting trend in the upper

zone is the similar increase in $\phi_{p,small}$ for L0 and L1 before the crossover at t = 145 s where they begin to diverge, with L0 rising higher than L1. This is perhaps due to the continued fallout of some particles closer to the 20 μm size threshold in L0, which make their way back from near the ceiling into the upper zone. In this zone, the effect of thermal stratification is less pronounced unless it is particularly strong as in case L2. Over longer time, the effect of weaker stratification may show a further reducing trend as indicated by the divergence between L0 and L1 in Fig. 11(b).

E. Particles reach over time

Figure 12 quantifies the reach of all three particle volume fractions—computed as described by Eq. (8)—at two time instants: 60 s [Fig. 12(a)] and 180 s [Fig. 12(b)]. The accumulated value of each fraction was computed in eight different vertical slices extracted in the YZ plane in increments of 0.5 m from the speaker, which cover the whole width and height of the room for L2 case. Stratification affects the height at which particles are found—since we are integrating along the whole vertical direction, the choice of case for this analysis is not as significant. Integration of $\phi_{p,small}$, $\phi_{p,medium}$, and $\phi_{p,large}$ at each slice was performed to obtain the respective particle volume fraction at the selected distance from the speaker. The concentrations were normalized by the volume fraction computed at x = 0.5 m and t = 180 s. Overall, droplets ($\phi_{p,large}$, red) are only present 0.5 m away from the speaker and do not reach the 1 m mark irrespective of time, demonstrating the inability of droplets to remain airborne due to their size. Medium particles ($\phi_{p,medium}$, green) can be found 2 m away from the speaker at 60 s and, in a very small amount, 2.5 m away from the speaker at 180 s. The small aerosol fraction ($\phi_{p,small}$, blue) reaches 3 m away from the speaker during the first minute within the simulation and 4 m within 3 min. While to the best of our knowledge, the exact concentration needed for infection is not yet known, the results in Fig. 12 show that aerosol particles, in particular, can travel large distances from the speaker and pose an infection risk both in close and far range of an infectious individual, while droplets do not travel very far. As earlier results indicate, e.g., Sec. V B, two people would have to stand very close together for particles in this size range to pose an infection risk assuming that both the infectious and susceptible individuals are standing face-to-face.

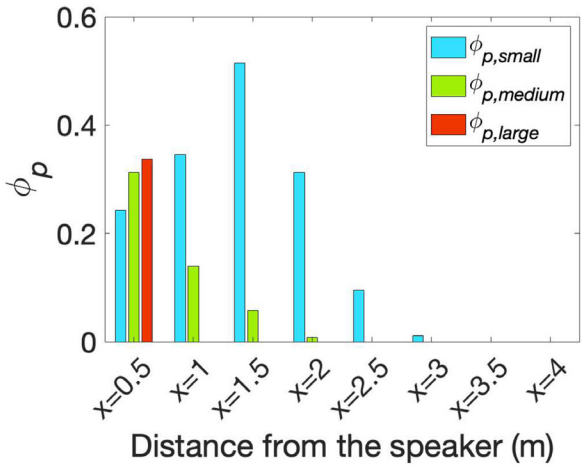

(a)

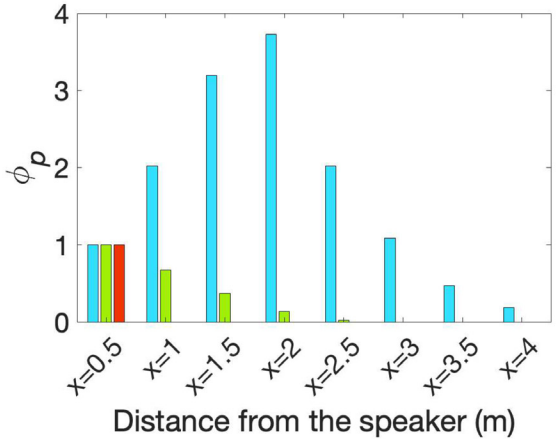

(b)

FIG. 12. Reach of differently sized particles at (a) 60 and (b) 180 s. The $\phi_{p,small}$, $\phi_{p,medium}$, and $\phi_{p,large}$ values in both figures were normalized by the respective fraction value found at x = 0.5 m and t = 180 s.

The small aerosol fraction ($\phi_{p,small}$, blue) exhibits a rather smooth distribution with maxima at x = 1.5 m after 1 min of simulation time and x = 2 m after 3 min [Figs. 12(a) and 12(b), respectively]. It is important to note that this is not an instantaneous concentration of particles—that would always be highest at the source. The variable $\phi_{p,small}$ is accumulative; hence, the presence of a particle can be recorded several times if it recirculates or lingers, increasing the risk of infection. Between 60 and 180 s, the smallest aerosols have traveled a further meter. More importantly, Fig. 12(b) shows that in the 120 s time difference between both figures, $\phi_{p,small}$ has increased significantly at all locations due to particles with $d_p \leq 20\,\mu m$ remaining airborne and accumulating as the person continues to speak. Interestingly, the reach of medium sized particles is largely unaffected by time as in both Figs. 12(a) and 12(b), they can be found 2 m away from the speaker—at t = 180 s, there is a very small amount present at x = 2.5 m.

VI. CONCLUSIONS

This work introduces a large-eddy simulation model coupled with a Eulerian–Lagrangian algorithm that computes the transport of realistic polydispersed expiratory particles released within an exhalation jet. The effect of thermal stratification on the behavior of the exhaled flow at room scale has been investigated. Our research considered three temperature gradients and two different room sizes to further analyze their effects on the particle dispersion pattern. Expiratory particles of different sizes were tracked individually in space and time, which allowed us to quantify their reach and analyze how their size interacted with the flow structures under different strengths of stratification. Particle volume fraction was tracked in space and time throughout the simulations and used to (1) quantify the accumulation of smallest aerosols in the near-field zone of the speaker and (2) illustrate how far from the speaker different sized categories of particles travel. The solver's ability to predict the exhalation jet's trajectory in isothermal and thermally stratified conditions has been validated against the non-dimensional theoretical buoyant jet dispersion model

developed by Zhou *et al.*[68] The numerical results show a good agreement with the predicted jet centerline trajectory. The mesh sensitivity analysis shows that the mesh resolution used in our simulations provides reliable results and does not overpredict the particle dispersion pattern.

The main findings of our study are as follows:

- thermal stratification effects become important after the jet begins its curvature—before this point, momentum dominates regardless of stratification effects;
- thermal stratification constrains the upward movement of the exhaled material, leading to an increase in the concentration of small aerosols at the breathing height, with this effect becoming stronger as temperature gradient increases;
- there exists a threshold between 12 and 20 μm aerosols whereby their behavior changes from locked-up by stratification to a continuous fall out from the exhalation jet;
- small aerosols can travel up to 4 m away from the speaker in all cases within 3 min, and their concentration increases significantly;
- medium aerosols are entrained in the exhalation cloud but detach due to their inertia gradually; their reach is within approximately 2 m downwards of the speaker and they do not accumulate;
- larger particles ($d_p > 60\,\mu$m) do not follow a ballistic trajectory, are unaffected by stratification, and their reach is within 0.5 m downwards of the speaker;
- in small rooms, walls act as barriers that induce a recirculating airflow, bringing exhaled material back toward the speaking person and increase dispersion in the room.

Our work has not considered ventilation effects, yet it has highlighted how critical this might be to mitigate infection risks. When strong thermal stratification occurs, the small aerosols can be trapped in an oscillating current at breathing height, increasing their concentration significantly, up to 27% when comparing our non-stratified and heavily stratified cases. Extraction of air from the upper layers of the room might not be effective due to the lock-up effect. This is an element of risk that can be addressed via a correct ventilation strategy that breaks the stratification layers. Our work shows that vertical temperature gradients acceptable from thermal comfort perspective may be unacceptable from a cross-infection perspective due to the lock-up effects discussed earlier.

ACKNOWLEDGMENTS

This research was supported by funding from the Engineering and Physical Sciences Research Council. The simulations were performed using computational resources provided by the UK National Supercomputing Service ARCHER2.

AUTHOR DECLARATIONS

Conflict of Interest

The authors have no conflicts to disclose.

Author Contributions

Aleksandra Monka: conceptualization (supporting); data curation (lead); formal analysis (equal); funding acquisition (supporting); investigation (lead); methodology (equal); project administration (supporting); resources (supporting); software (supporting); validation (lead); visualization (lead); writing—original draft (lead); and writing—review and editing (supporting). **Bruño Fraga:** conceptualization (lead); formal analysis (equal); funding acquisition (lead); investigation (supporting); methodology (equal); project administration (lead); resources (lead); software (lead); supervision (lead); validation (supporting); visualization (supporting); and writing—review and editing (lead). **David Soper:** supervision (supporting) and writing—review and editing (supporting). **Hassan Hemida:** funding acquisition (supporting); resources (supporting); and supervision (supporting).

DATA AVAILABILITY

The data that support the findings of this study are available from the corresponding author upon reasonable request.

REFERENCES

[1]L. Bourouiba, E. Dehandschoewercker, and J. W. Bush, "Violent expiratory events: On coughing and sneezing," J. Fluid Mech. **745**, 537–563 (2014).
[2]L. Bourouiba, "The fluid dynamics of disease transmission," Annu. Rev. Fluid Mech. **53**, 473 (2021).
[3]J. W. Tang, W. P. Bahnfleth, P. M. Bluyssen, G. Buonanno, J. L. Jimenez, J. Kurnitski, Y. Li, S. Miller, C. Sekhar, L. Morawska *et al.*, "Dismantling myths on the airborne transmission of severe acute respiratory syndrome coronavirus (SARS-CoV-2)," J. Hosp. Infect. **110**, 89 (2021).
[4]L. C. Marr and J. W. Tang, "A paradigm shift to align transmission routes with mechanisms," Clin. Infect. Dis. **73**, 1747–1749 (2021).
[5]L. Morawska and J. Cao, "Airborne transmission of SARS-CoV-2: The world should face the reality," Environ. Int. **139**, 105730 (2020).
[6]F. C. Fang, C. A. Benson, C. Del Rio, K. M. Edwards, V. G. Fowler, Jr., D. N. Fredricks, A. P. Limaye, B. E. Murray, S. Naggie, P. G. Pappas *et al.*, "COVID-19–Lessons learned and questions remaining," Clin. Infect. Dis. **72**, 2225 (2021).
[7]W. Chen, N. Zhang, J. Wei, H.-L. Yen, and Y. Li, "Short-range airborne route dominates exposure of respiratory infection during close contact," Build. Environ. **176**, 106859 (2020).
[8]G. Cortellessa, L. Stabile, F. Arpino, D. Faleiros, W. Van Den Bos, L. Morawska, and G. Buonanno, "Close proximity risk assessment for SARS-CoV-2 infection," Sci. Total Environ. **794**, 148749 (2021).
[9]Y. Li, H. Qian, J. Hang, X. Chen, P. Cheng, H. Ling, S. Wang, P. Liang, J. Li, S. Xiao *et al.*, "Probable airborne transmission of SARS-CoV-2 in a poorly ventilated restaurant," Build. Environ. **196**, 107788 (2021).
[10]J. Shen, M. Kong, B. Dong, M. J. Birnkrant, and J. Zhang, "Airborne transmission of SARS-CoV-2 in indoor environments: A comprehensive review," Sci. Technol. Built Environ. **27**, 1331–1367 (2021).
[11]E. L. Anderson, P. Turnham, J. R. Griffin, and C. C. Clarke, "Consideration of the aerosol transmission for COVID-19 and public health," Risk Anal. **40**, 902 (2020).
[12]T. Greenhalgh, J. L. Jimenez, K. A. Prather, Z. Tufekci, D. Fisman, and R. Schooley, "Ten scientific reasons in support of airborne transmission of SARS-CoV-2," Lancet **397**, 1603–1605 (2021).
[13]S. Tang, Y. Mao, R. M. Jones, Q. Tan, J. S. Ji, N. Li, J. Shen, Y. Lv, L. Pan, P. Ding *et al.*, "Aerosol transmission of SARS-CoV-2? Evidence, prevention and control," Environ. Int. **144**, 106039 (2020).
[14]R. Tellier, "COVID-19: The case for aerosol transmission," Interface Focus **12**, 20210072 (2022).
[15]M. Schifko, A. Eslamian, V. Maurya, A. Stadik, E. Monaco, R. Singh, J. Basic, D. Dietrich, A. Hinterreiter, J. Jindra *et al.*, "On the democratization of the fluid flow simulation," in Proceedings of the 8th World Congress on New Technologies (2022).
[16]C. Crawford, E. Vanoli, B. Decorde, M. Lancelot, C. Duprat, C. Josserand, J. Jilesen, L. Bouadma, and J.-F. Timsit, "Modeling of aerosol transmission of

airborne pathogens in ICU rooms of COVID-19 patients with acute respiratory failure," Sci. Rep. **11**, 11778 (2021).
[17]M. Beaussier, E. Vanoli, F. Zadegan, H. Peray, E. Bezian, J. Jilesen, G. Gandveau, and J.-M. Gayraud, "Aerodynamic analysis of hospital ventilation according to seasonal variations. A simulation approach to prevent airborne viral transmission pathway during COVID-19 pandemic," Environ. Int. **158**, 106872 (2022).
[18]N. Salman, A. Khan, A. Kemp, and C. Noakes, "Indoor temperature forecast based on the lattice Boltzmann method and data assimilation," Build. Environ. **210**, 108654 (2022).
[19]M. Abuhegazy, K. Talaat, O. Anderoglu, and S. V. Poroseva, "Numerical investigation of aerosol transport in a classroom with relevance to COVID-19," Phys. Fluids **32**, 103311 (2020).
[20]T. G. Foat, B. Higgins, C. Abbs, T. Maishman, S. Coldrick, A. Kelsey, M. J. Ivings, S. T. Parker, and C. J. Noakes, "Modeling the effect of temperature and relative humidity on exposure to SARS-CoV-2 in a mechanically ventilated room," Indoor Air **32**, e13146 (2022).
[21]L. Liu, Y. Li, P. V. Nielsen, J. Wei, and R. L. Jensen, "Short-range airborne transmission of expiratory droplets between two people," Indoor Air **27**, 452–462 (2017).
[22]Z. Zhang, T. Han, K. H. Yoo, J. Capecelatro, A. L. Boehman, and K. Maki, "Disease transmission through expiratory aerosols on an urban bus," Phys. Fluids **33**, 015116 (2021).
[23]S. Coldrick, A. Kelsey, M. J. Ivings, T. G. Foat, S. T. Parker, C. J. Noakes, A. Bennett, H. Rickard, and G. Moore, "Modeling and experimental study of dispersion and deposition of respiratory emissions with implications for disease transmission," Indoor Air **32**, e13000 (2022).
[24]S. Shao, D. Zhou, R. He, J. Li, S. Zou, K. Mallery, S. Kumar, S. Yang, and J. Hong, "Risk assessment of airborne transmission of COVID-19 by asymptomatic individuals under different practical settings," J. Aerosol Sci. **151**, 105661 (2021).
[25]R. R. Rajendran, F. E. Ţurcanu, R. Tawfiqur, and H. Askarpour, "Computational fluid dynamic analysis of corona virus patients breathing in an airplane," Phys. Fluids **35**, 035129 (2023).
[26]C. Wang and J. Hong, "Numerical investigation of airborne transmission in low-ceiling rooms under displacement ventilation," Phys. Fluids **35**, 023321 (2023).
[27]J. Komperda, A. Peyvan, D. Li, B. Kashir, A. L. Yarin, C. M. Megaridis, P. Mirbod, I. Paprotny, L. F. Cooper, S. Rowan *et al.*, "Computer simulation of the SARS-CoV-2 contamination risk in a large dental clinic," Phys. Fluids **33**, 033328 (2021).
[28]S. Salim, K. Ong, and S. Cheah, "Comparison of RANS, URANS and LES in the prediction of airflow and pollutant dispersion," in Proceedings of the World Congress on Engineering and Computer Science (2011), Vol. 2, pp. 19–21.
[29]W. Rodi, G. Constantinescu, and T. Stoesser, *Large-Eddy Simulation in Hydraulics* (CRC Press, 2013).
[30]Z. Zhang, W. Zhang, Z. J. Zhai, and Q. Y. Chen, "Evaluation of various turbulence models in predicting airflow and turbulence in enclosed environments by CFD: Part 2—Comparison with experimental data from literature," HVAC&R Res. **13**, 871–886 (2007).
[31]M. Wang and Q. Chen, "Assessment of various turbulence models for transitional flows in an enclosed environment (RP-1271)," HVAC&R Res. **15**, 1099–1119 (2009).
[32]V. Vuorinen, M. Aarnio, M. Alava, V. Alopaeus, N. Atanasova, M. Auvinen, N. Balasubramanian, H. Bordbar, P. Erästö, R. Grande *et al.*, "Modelling aerosol transport and virus exposure with numerical simulations in relation to SARS-CoV-2 transmission by inhalation indoors," Saf. Sci. **130**, 104866 (2020).
[33]M. Abkarian, S. Mendez, N. Xue, F. Yang, and H. A. Stone, "Speech can produce jet-like transport relevant to asymptomatic spreading of virus," Proc. Natl. Acad. Sci. **117**, 25237–25245 (2020).
[34]M. Auvinen, J. Kuula, T. Grönholm, M. Sühring, and A. Hellsten, "High-resolution large-eddy simulation of indoor turbulence and its effect on airborne transmission of respiratory pathogens-model validation and infection probability analysis," Phys. Fluids **34**, 015124 (2022).
[35]K. Liu, M. Allahyari, J. Salinas, N. Zgheib, and S. Balachandar, "Investigation of theoretical scaling laws using large eddy simulations for airborne spreading of viral contagion from sneezing and coughing," Phys. Fluids **33**, 063318 (2021).
[36]L. K. Norvihoho, H. Li, Z.-F. Zhou, J. Yin, S.-Y. Chen, D.-Q. Zhu, and B. Chen, "Dispersion of expectorated cough droplets with seasonal influenza in an office," Phys. Fluids **35**, 083302 (2023).
[37]C. Peña-Monferrer, S. Antao, and R. Manson-Sawko, "Numerical investigation of droplets in a cross-ventilated space with sitting passengers under asymptomatic virus transmission conditions," Phys. Fluids **33**, 123314 (2021).
[38]K. Monroe, Y. Yao, A. Lattanzi, V. Raghav, and J. Capecelatro, "Role of pulsatility on particle dispersion in expiratory flows," Phys. Fluids **33**, 043311 (2021).
[39]K. L. Chong, C. S. Ng, N. Hori, R. Yang, R. Verzicco, and D. Lohse, "Extended lifetime of respiratory droplets in a turbulent vapor puff and its implications on airborne disease transmission," Phys. Rev. Lett. **126**, 034502 (2021).
[40]A. Giri, N. Biswas, D. L. Chase, N. Xue, M. Abkarian, S. Mendez, S. Saha, and H. A. Stone, "Colliding respiratory jets as a mechanism of air exchange and pathogen transport during conversations," J. Fluid Mech. **930**, R1 (2022).
[41]A. Fabregat, F. Gisbert, A. Vernet, S. Dutta, K. Mittal, and J. Pallarès, "Direct numerical simulation of the turbulent flow generated during a violent expiratory event," Phys. Fluids **33**, 035122 (2021).
[42]J. Pallares and A. Fabregat, "A model to predict the short-term turbulent indoor dispersion of small droplets and droplet nuclei released from coughs and sneezes," Indoor Built Environ. **31**, 1393 (2022).
[43]A. C. Lai and F. Chen, "Comparison of a new Eulerian model with a modified Lagrangian approach for particle distribution and deposition indoors," Atmos. Environ. **41**, 5249–5256 (2007).
[44]M.-R. Pendar and J. C. Páscoa, "Numerical modeling of the distribution of virus carrying saliva droplets during sneeze and cough," Phys. Fluids **32**, 083305 (2020).
[45]P. V. Nielsen, I. Olmedo, M. R. de Adana, P. Grzelecki, and R. L. Jensen, "Airborne cross-infection risk between two people standing in surroundings with a vertical temperature gradient," HVAC&R Res. **18**, 552–561 (2012).
[46]F. Liu, H. Qian, Z. Luo, S. Wang, and X. Zheng, "A laboratory study of the expiratory airflow and particle dispersion in the stratified indoor environment," Build. Environ. **180**, 106988 (2020).
[47]G. Pei, M. Taylor, and D. Rim, "Human exposure to respiratory aerosols in a ventilated room: Effects of ventilation condition, emission mode, and social distancing," Sustainable Cities Soc. **73**, 103090 (2021).
[48]H. Liu, S. He, L. Shen, and J. Hong, "Simulation-based study of COVID-19 outbreak associated with air-conditioning in a restaurant," Phys. Fluids **33**, 023301 (2021).
[49]A. C. Lai and S.-L. Wong, "Experimental investigation of exhaled aerosol transport under two ventilation systems," Aerosol Sci. Technol. **44**, 444–452 (2010).
[50]A. Lai and S. L. Wong, "Expiratory aerosol transport in a scaled chamber under a variety of emission characteristics: An experimental study," Aerosol Sci. Technol. **45**, 909–917 (2011).
[51]E. Bjùrn and P. V. Nielsen, "Dispersal of exhaled air and personal exposure in displacement ventilated rooms," Indoor Air **12**, 147–164 (2002).
[52]R. K. Bhagat, M. D. Wykes, S. B. Dalziel, and P. Linden, "Effects of ventilation on the indoor spread of COVID-19," J. Fluid Mech. **903**, F1 (2020).
[53]M. Möhlenkamp, M. Schmidt, M. Wesseling, A. Wick, I. Gores, and D. Müller, "Thermal comfort in environments with different vertical air temperature gradients," Indoor air **29**, 101–111 (2019).
[54]B. Fraga, T. Stoesser, C. C. Lai, and S. A. Socolofsky, "A LES-based Eulerian–Lagrangian approach to predict the dynamics of bubble plumes," Ocean Modell. **97**, 27–36 (2016).
[55]B. Fraga and T. Stoesser, "Influence of bubble size, diffuser width, and flow rate on the integral behavior of bubble plumes," J. Geophys. Res. **121**, 3887–3904, https://doi.org/10.1002/2015JC011381 (2016).
[56]C. C. Lai, B. Fraga, W. Chan, and M. S. Dodd, "Energy cascade in a homogeneous swarm of bubbles rising in a vertical channel," in *Proceedings of the Summer Program, Center for Turbulence Research* [Center for Turbulence Research (CTR), Stanford University, 2018], pp. 55–64.
[57]B. Chen, B. Fraga, and H. Hemida, "Large-eddy simulation of enhanced mixing with buoyant plumes," Chem. Eng. Res. Des. **177**, 394–405 (2022).
[58]I. Paul, B. Fraga, M. S. Dodd, and C. Lai, "The role of breakup and coalescence in fine-scale bubble-induced turbulence—I: Dynamics," Phys. Fluids **34**, 083321 (2022).
[59]B. Chen, B. Fraga, and H. Hemida, "A three-phase Eulerian–Lagrangian model to simulate mixing and oxygen transfer in activated sludge treatment," Int. J. Multiphase Flow **168**, 104555 (2023).

[60]C. S. Peskin, "The immersed boundary method," Acta Numer. **11**, 479–517 (2002).
[61]E. Delnoij, F. Lammers, J. Kuipers, and W. P. M. van Swaaij, "Dynamic simulation of dispersed gas-liquid two-phase flow using a discrete bubble model," Chem. Eng. Sci. **52**, 1429–1458 (1997).
[62]R. Clift, J. R. Grace, and M. E. Weber, *Bubbles, Drops, and Particles* (Dover Publications, Inc., New York, 2005).
[63]C. Crowe, M. Sommerfeld, and Y. Tsuji, *Multiphase Flows with Droplets and Particles* (CRC Press, 1998).
[64]J. Duguid, "The size and the duration of air-carriage of respiratory droplets and droplet-nuclei," Epidemiol. Infect. **44**, 471–479 (1946).
[65]A. Hartmann, J. Lange, H. Rotheudt, and M. Kriegel, "Emission rate and particle size of bioaerosols during breathing, speaking and coughing" (Technische Universität Berlin, 2020).
[66]J. K. Gupta, C.-H. Lin, and Q. Chen, "Characterizing exhaled airflow from breathing and talking," Indoor Air **20**, 31–39 (2010).
[67]C. Xu, P. Nielsen, G. Gong, L. Liu, and R. Jensen, "Measuring the exhaled breath of a manikin and human subjects," Indoor Air **25**, 188–197 (2015).
[68]Q. Zhou, H. Qian, H. Ren, Y. Li, and P. V. Nielsen, "The lock-up phenomenon of exhaled flow in a stable thermally-stratified indoor environment," Build. Environ. **116**, 246–256 (2017).
[69]H. Qian, Y. Li, P. V. Nielsen, C.-E. Hyldgaard, T. W. Wong, and A. Chwang, "Dispersion of exhaled droplet nuclei in a two-bed hospital ward with three different ventilation systems," Indoor Air **16**, 111–128 (2006).
[70]F. Liu, C. Zhang, H. Qian, X. Zheng, and P. V. Nielsen, "Direct or indirect exposure of exhaled contaminants in stratified environments using an integral model of an expiratory jet," Indoor Air **29**, 591–603 (2019).